


AUTHOR QUERY FORM

 ELSEVIER	Journal: ENSO Article Number: 2986	Please e-mail or fax your responses and any corrections to: E-mail: corrections.esch@elsevier.tnq.co.in Fax: +31 2048 52789
--	---	---

Dear Author,

Please check your proof carefully and mark all corrections at the appropriate place in the proof (e.g., by using on-screen annotation in the PDF file) or compile them in a separate list. Note: if you opt to annotate the file with software other than Adobe Reader then please also highlight the appropriate place in the PDF file. To ensure fast publication of your paper please return your corrections within 48 hours.

For correction or revision of any artwork, please consult <http://www.elsevier.com/artworkinstructions>.

Any queries or remarks that have arisen during the processing of your manuscript are listed below and highlighted by flags in the proof.

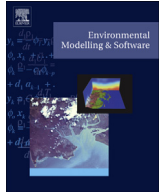
Location in article	Query / Remark: Click on the Q link to find the query's location in text Please insert your reply or correction at the corresponding line in the proof
Q1	Please check the address for the corresponding author that has been added here, and correct if necessary.
Q2	Please provide the volume number and page range for the references Jerosch, 2012; Bennett et al., 2012; Fuller and Basher, 2012 and Legleiter, 2012.
Q3	Please update Liu et al., 2012.
Q4	Please update Shelley et al., 2013.
Q5	Please confirm that given names and surnames have been identified correctly.
	<div data-bbox="304 1332 895 1513"> <p>Please check this box or indicate your approval if you have no corrections to make to the PDF file</p> <input data-bbox="791 1391 879 1476" type="checkbox"/> </div>

Thank you for your assistance.



Contents lists available at ScienceDirect

Environmental Modelling & Software

journal homepage: www.elsevier.com/locate/envsoft

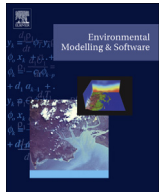
Highlights

- A method for bathymetry fusion using multiple-point geostatistics is presented.
- An approach to capture nonstationarity in bedforms is discussed.
- High resolution bathymetry is simulated at the frequency of the low-resolution data.
- This is a cost-effective alternative to periodic detailed survey of bathymetry.



Contents lists available at ScienceDirect

Environmental Modelling & Software

journal homepage: www.elsevier.com/locate/envsoft

Bathymetry fusion using multiple-point geostatistics: Novelty and challenges in representing non-stationary bedforms

Q5 **Sanjeev Kumar Jha^{a, b, *}, Gregoire Mariethoz^{a, b}, Bryce F.J. Kelly^{a, b}**^a Connected Waters Initiative Research Centre, University of New South Wales, Sydney, NSW, Australia^b National Centre for Groundwater Research & Training, Australia

ARTICLE INFO

Article history:

Received 11 December 2012

Received in revised form

14 May 2013

Accepted 2 September 2013

Available online xxx

Keywords:

Bathymetry

Geostatistics

Multiple-point geostatistics

Direct sampling

Bedforms

ABSTRACT

In large rivers, complex sediment dynamics cause rapid changes in the position and shape of bed deposits. Regular monitoring of changes in river bed geometry is essential for assessing the nature of morphological change and associated bed load during low, high, and medium flow conditions. We demonstrate the application of Direct Sampling (DS) for patching partial river morphological surveys to generate complete maps of the river morphology, by incorporating prior knowledge from bathymetry data collected in different seasons at collocated or adjacent reaches. This novel approach is based on multiple-point statistics (MPS), which uses a training image (TI) to provide prior statistical and architectural constraining data. In this study high and low resolution bathymetry data from a reach of the Mississippi river have been used. High-resolution measurements were conducted using Multi-beam-echo-sounder (MBES), which provides very detailed bed geometry at high spatial resolution. These measurements cannot be acquired at intervals frequent enough to characterize the rapid sedimentological processes. Low resolution bathymetry data can be obtained at frequent intervals but at sparse locations, by installing depth measuring sensors on boats passing the study reach several times a week. The DS method is used to simulate the high resolution bathymetry at the frequency of the low-resolution data. In the simulations, the method uses the bed geometry information contained in the MBES high-resolution surveys, the local information contained in the boat-borne low-resolution measurements, and provides an updated bathymetry map with quantified uncertainty.

© 2013 Published by Elsevier Ltd.

1. Introduction

Accurate estimation of bathymetry is necessary for evaluating changes in river-channel morphology (Fonstad and Marcus, 2010), determining reservoir volume (Furnans and Austin, 2008), water quality modelling (Mantas et al., 2011), providing boundary conditions for numerical modelling of flow dynamics and sediment transport (Liu et al., 2012), and for measuring the movement of sediment in the waterway (Jiang et al., 2011). The impact of sediment dynamics on spatio-temporal patterns of erosion and deposition is evaluated by observing the differences in digital elevation models, which are created from repeat bathymetric surveys (Fuller and Basher, 2012).

In shallow rivers and coastal areas, there is growing interest in using remote sensing to accurately estimate the bathymetry (Legleiter and Roberts, 2009). A variety of measurement tools for remote bathymetry surveying are available, including satellite imagery (Stumpf et al., 2003), LiDAR technology (Bailly et al., 2010) or a combination of these methods (Coleman et al., 2011; Legleiter, 2012). However, these methods fail to retrieve the bathymetry of deep and turbid rivers. In such cases, Multi-beam-echo-sounder (MBES) sonar systems have been employed in recent decades to measure the bed morphology in oceans, deep lakes and rivers (Simmons et al., 2007). MBES has the advantage of covering large areas with each individual LASER pulse, or ping of sound, and thus scans distinguishable morphological patterns at the river bottom at high-accuracy and high-resolution spatial scales (Costa et al., 2009; Cutter et al., 2003; Masetti and Calder, 2012). In large rivers, the bed shape can change rapidly as a consequence of morphodynamic processes. Accurately and efficiently keeping track of the changes in bathymetry requires frequent detailed surveys. Although MBES

Q1 * Corresponding author. Connected Waters Initiative Research Centre, University of New South Wales, Sydney, NSW, Australia.

E-mail addresses: s.jha@unsw.edu.au, jha.sanj@gmail.com (S.K. Jha).

provides high-resolution data, the high cost prevents its regular use (Quinn and Boland, 2010). The alternate option of Single-beam-echo-sounders (SBES) bathymetry surveying is inexpensive and can be used to rapidly obtain low-resolution data. However, SBES provides inadequate gap-free data (Jena et al., 2012). An economically feasible option is to conduct detailed surveys at specific intervals, for example after extreme events, and then update the maps using low resolution but cost-effective data.

Various methods have been proposed to integrate bathymetry data from multiple sources including bathymetry fusion (Elmore and Steed, 2008) or bathymetry merging (Gesch and Wilson, 2002). Merging or fusion of bathymetry data has been used to improve the resolution of a historical topography map with satellite imagery (Alcântara et al., 2010), to combine observation of two satellites (Sindhu et al., 2007) and to enhance satellite imagery with bathymetry data obtained from LiDAR (Calder, 2006; Wozencraft and Millar, 2005). However, to the best of our knowledge, there is a scarcity of approaches for updating high-resolution infrequent bathymetry surveys with more frequent but lower resolution data. This is a challenging problem because it involves integrating data types of a very different nature. The infrequent high-resolution surveys provide accurate bed feature information such as the shape and size of the sand bars, the spatial frequency of their occurrence or the spatial continuity of deeper areas. However, the local information in these surveys is quite weak. Given the rapid changes in the river bathymetry, any survey no matter how accurate is likely to be outdated in a couple of months (or days during high flow periods). The boat-mounted acoustic measurements (SBDM) are frequent enough to be locally accurate; however they only cover a limited area. Therefore, it would be desirable to have the ability to extract the bed feature properties of the MBES data, and adapt them such that locally they correspond to the SBDM measured values. Ideally, away from these measurements the bathymetry should still present a similar spatial morphology and bed features as observed in the MBES survey, but with an associated uncertainty due to the lack of local information.

Geostatistics is a natural tool for analyzing spatially correlated variables. Ordinary kriging is commonly used in interpolating river channel bathymetry to obtain bed topography (Carter and Shankar, 1997; Chappell et al., 2003; Legleiter and Kyriakidis, 2008; Merwade, 2009; Merwade et al., 2006). Cokriging algorithms have been applied in the mapping of bedforms by considering bathymetry, slope, and sediment input (Jerosch, 2012). Using such approaches, the integration of newly measured data to the already developed base map would require the updating of variogram parameters (Barnes and Watson, 1992) and kriging to obtain an updated surface (Jha et al., 2011). However a fundamental issue is that kriging is based on linear geostatistics, which assumes that the mean and variance of the increments are spatially stationary (Goovaerts, 1997), and provides smooth interpolated values at unsampled locations by giving more weight to local neighborhood data than the global statistical properties (Journal and Huijbregts, 1978). More generally, linear geostatistics are not designed to represent low entropy patterns and salient features such as those formed by river flow mechanisms (Journal and Zhang, 2006). A detailed representation of bathymetry patterns is however critical because these patterns exert a strong influence on sediment transport (Shelley et al., 2013), and control the flow mechanisms in and out of the river bed (Gooseff et al., 2006). The smoothed representation typical of kriging approaches is therefore not appropriate for certain types of applications.

The issue of smoothing with kriging and the need to represent specific patterns motivated the development of multiple-point

geostatistics (MPS) (Guardiano and Srivastava, 1993). MPS is a non-parametric approach, and as such it is free from linearity or multi-Gaussianity assumptions (Gómez-Hernández and Wen, 1998). The main feature of MPS is that it uses training images to describe complex patterns of spatial continuity. In this paper we solve the integration of bathymetry data collected at different resolutions and at different time periods using an approach based on MPS.

Most MPS techniques derive arrangements of values from a training image and store them in a database (Strebel, 2002). The database is then used to retrieve the conditional probabilities for the simulation. Early MPS methods such as SNESIM (Strebel, 2002) were aimed at simulating categorical variables, for example geological facies or land use classes (Boucher et al., 2008; Feyen and Caers, 2006). However, recent MPS algorithms such as SIMPAT (Arpat and Caers, 2007), FILTERSIM (Zhang, 2006), and Direct Sampling (Mariethoz et al., 2010) allow for the use of continuous variables like bathymetry. In this paper, we use Direct Sampling (DS), which compared to other continuous-variable based MPS methods, has a number of advantages relevant for applications to bathymetry:

- 1) It does not require a database of patterns, and is therefore memory efficient and can handle very large data sets;
- 2) It is very effective for data conditioning because it does not use systems such as data templates or multiple-grids, which require approximations on the conditioning data locations; and
- 3) It allows using multivariate training images, and this possibility can be used to take into account complex non-stationarity, which is a common feature for bathymetry data.

Recently, DS has been successfully applied in the stochastic downscaling of climate models (Jha et al., 2013), the completion of partially-informed remote sensing images (Mariethoz et al., 2012) and the incorporation of prior geological concepts in subsurface models (Mariethoz and Kelly, 2011). In this study DS is used to merge the infrequent detailed information contained in MBES bathymetric surveys and data collected at a higher frequency but with partial coverage by boat-borne surveys. Patterns contained in MBES data recorded during the highest and lowest river-flows are used as training images. The patterns in those training images are conditioned to the more recently acquired SBDM data, which results in an updated map of bathymetry that is accurate at the sparse locations measured at high frequency, and which honors the patterns observed in the detailed but infrequent MBES surveys. To the best of our knowledge, this is the first time two equiprobable training images have been used in a DS simulation to provide the complete range of values for a single intermediate state.

2. Methodology

The methodology adopted to update the river bathymetry is based on the Direct Sampling (DS) geostatistical simulation approach. It generates realizations of a variable Z that present the same spatial continuity as a given training image, and given conditioning data. The inputs are therefore a training image, a simulation grid, and a set of conditioning data. The nodes of the simulation grid are visited sequentially in a random order. For each simulation grid node, the pattern formed by the neighboring values is defined, and the training image is sampled to find a representative location having a similar neighborhood. The value at this representative location is then pasted in the simulation grid.

In an algorithmic form, the DS algorithm is summarized below:

Input: (a) Simulation grid SG with locations denoted \mathbf{x} , (b) training image TI with locations denoted \mathbf{y} , (c) conditioning data, (d) distance function $d(\cdot)$ bounded in $[0,1]$, (e) distance threshold t (distance under which two neighborhoods are considered identical).

1. Migrate conditioning data to SG.
2. **while** # non-informed locations in SG > 0 **do**
3. Choose a non-informed location \mathbf{x} in SG and identify the neighborhood \mathbf{N}_x centered on \mathbf{x} .
4. Initialize $d(\mathbf{N}_x, \mathbf{N}_y) = \infty$
5. **while** $d(\mathbf{N}_x, \mathbf{N}_y) \geq t$ **do**
6. Sample a location \mathbf{y} in TI.
7. Define \mathbf{N}_y as the neighborhood centered on \mathbf{y} having identical lag vectors as \mathbf{N}_x .
8. Compute the distance $d(\mathbf{N}_x, \mathbf{N}_y)$.
9. **end while**
10. Assign $Z(\mathbf{x}) = Z(\mathbf{y})$
11. **end while**

Output: Completed simulation SG

For continuous variables, the distance adopted is a normalized Manhattan distance computed over the nodes in both neighborhoods:

$$d(\mathbf{N}_x, \mathbf{N}_y) = \frac{1}{n} \sum_{i=1}^n \frac{|Z(\mathbf{x}_i) - Z(\mathbf{y}_i)|}{\max_{y \in \Pi} Z(y) - \min_{y \in \Pi} Z(y)} \quad (1)$$

where n is the number of nodes in the neighborhoods being compared. The main principle is that once a first matching neighborhood is found (i.e., when $d(\mathbf{N}_x, \mathbf{N}_y) < t$), the corresponding value $Z(\mathbf{y})$ is a sample of the conditional distribution $\text{Prob}[Z(\mathbf{x})|\mathbf{N}_x]$, and the search can be interrupted, therefore saving computing time.

The result is a realization of Z that contains the same spatial patterns (neighborhoods) as in the training image, and that is coherent with the conditioning data initially set in the simulation grid. When non-stationarity is present, locational variable control is added (Chugunova and Hu, 2006) to guide the search for a suitable matching pattern. In this case, a joint distance is defined for the variable Z and the locational variables together:

$$d_{\text{joint}}(\mathbf{N}_x, \mathbf{N}_y) = \sum_{k=1}^m w_k d(\mathbf{N}_x^k, \mathbf{N}_y^k) \quad (2)$$

where w is the weight used for linear combination of individual distances for each variable k , $k = 1 \dots m$. The sum total of all weights is 1. The detailed description of the DS algorithm is presented in Mariethoz et al. (2010) and applications to non-stationary modeling can be found in Jha et al. (2013).

3. Study area and available data

The study area is a seven-kilometer reach of the Mississippi river near Saint Louis, Missouri. The average width of the river channel on this reach is 720 m. The data used in this study come from river surveys conducted by the collaborative effort between the United States Geological Survey (USGS) at the Illinois Water Science Center and the University of Illinois Urbana-Champaign. The objective of these surveys was to assess the nature of the bed morphology between high-flow, low-flow, and medium-flow periods. Three MBES surveys (MBES1, MBES2 and MBES3) were conducted on 2nd April 2010, 4th November 2010, and 21st April 2011 when the river discharge measured at USGS St. Louis gage were $15,000 \text{ m}^3 \text{ s}^{-1}$ (high flow), $5800 \text{ m}^3 \text{ s}^{-1}$ (low flow), and $12,400 \text{ m}^3 \text{ s}^{-1}$ (medium flow) respectively (gage number 07010000). At the same time as the MBES3 survey, a single-beam depth measurement (SBDM) was also collected by installing two Doppler sensors on a boat traveling through the study reach. Both MBES and SBDM measurements consist of latitude (x), longitude (y), and depth (z) values. The study reach and sample of MBES and SBDM measurements are shown in Fig. 1.

It is important to note that the surveys MBES1, MBES2 and MBES3 were conducted during high, low and medium flow periods. An assumption that we make in this study is that in the intermediate river stage, one can expect to find patterns that are also present in both high and low flow regimes. We therefore consider that the statistical properties of the bedforms in MBES3 are somewhat intermediate between the other two survey data. In this case the SBDM data are biased and therefore do not allow validating our assumption. However, having all three surveys available, we can compare the histogram plots of MBES1, MBES2, and MBES3 at the SBDM locations. These are presented in Fig. 2a, with the histogram of MBES3 lying in-between the histograms of MBES1 and MBES2.

Since MBES3 and SBDM data were collected on the same day, we expect them to be similar at the measurement locations of SBDM. However, a systematic bias in the SBDM data was observed, which is due to the imprecision of the boat-borne measurement, as compared to the more accurate MBES data. Therefore it becomes necessary to correct the bias in the SBDM data by applying an affine transformation such that it becomes statistically similar as the MBES1 and MBES2 data. The following transformation is used to this end:

$$z'_{\text{SBDM}} = \frac{z_{\text{SBDM}} - \mu_{\text{SBDM}} \cdot \sigma_{\text{MBES1}} + \sigma_{\text{MBES2}}}{\sigma_{\text{SBDM}}} + \frac{\mu_{\text{MBES1}} + \mu_{\text{MBES2}}}{2} \quad (3)$$

where z represents the depth. The subscript in the terms indicates the measuring devices used for data collection. μ and σ represent the mean and standard deviation of z taken only at the locations where the SBDM boat survey is available. The transformed SBDM was used in our subsequent analysis. In Fig. 2b, we present the histogram plots of MBES3, SBDM and transformed SBDM obtained from Eq. (3). The mean values and standard deviation of MBES and SBDM data are presented in Table 1.

4. Application of DS for bathymetry updating

Two training images, from the MBES1 and MBES2 measurements at a resolution of 5 m, are shown in Fig. 3a and b respectively. MBES3 (reference bathymetry for the medium flow level) is shown in Fig. 3c. In MPS studies, commonly one training image is used to represent the variation in spatial structure. The assumption is that the information contained in the chosen training image contains

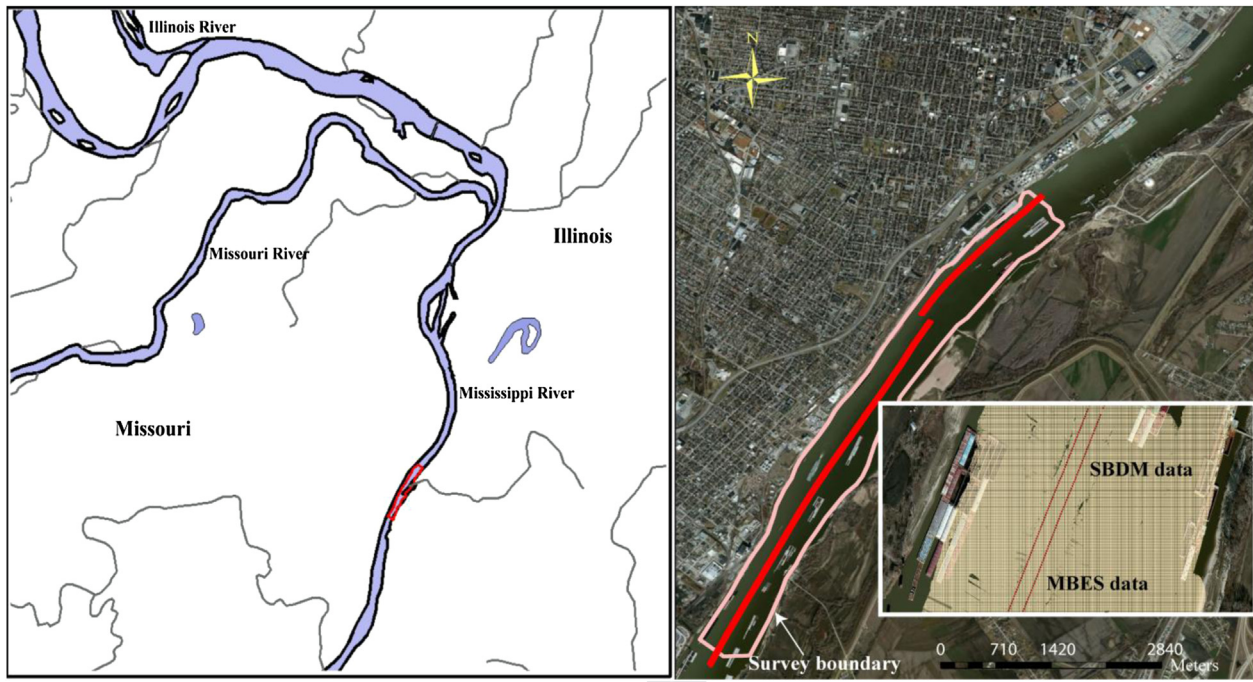


Fig. 1. Map showing the 7 km long study reach near Saint Louis, Missouri (left). The right side of the figure shows the zoomed-in section of the study reach with its boundary in pink color. The small figure indicates MBES measurements shown in light yellow color; and the points shown in red color indicate the SBDM measurement along the boat path. The data for the SBDM comes from two sensors installed on a boat. (For interpretation of the references to color in this figure legend, the reader is referred to the web version of this article.)

physical properties covering the primary processes under investigation. In the present study, the bed features in high and low flow change widely and it is impossible to present all the information in one training image. Therefore we use MBES1 and MBES2 as two equiprobable training images covering a wide range of possible bed features. From these figures, it can be observed that the bed morphology of the reach is non-stationary, showing relatively shallow areas adjacent to the east bank. The west bank is generally stable while the east bank is subjected to scour. The channel contains structures called dikes that are located on both east and west banks. These dikes are constructed to maintain adequate depth in the river; they extend from the bank into the water and prevent the buildup of sediment due to settling. This is visible in Fig. 3a–c as yellow lineations on the left bank. The channel is considerably deeper on the outside of the bend along the western bank of the river and the deepest point in the study reach is located in the region of flow constriction towards the lower part of the reach.

The trend in bedforms requires additional variables to be defined to account for non-stationarity. Due to the large variation in topographic features, a constraint has to be applied in the DS simulation to prevent bedforms coming from one environment (e.g. shallow bend interior) being used in a completely different environment (e.g. deep bend exterior). We evaluated scenarios imposing local consistency by including latitude (x), longitude (y) of the data point in the training image (Honarkhah and Caers, 2010) and by including an auxiliary variable, dl , the distance of points from the left boundary (Straubhaar et al., 2011). Thus, the training images contain four variables: x , y , bathymetry, and dl , and the importance of the three locational variables (x , y , dl) can be set using weights (w_x , w_y , and w_{dl}), which are used in Eq. (2). It is expected that along the main flow path, the bedforms will change in a similar manner. Therefore the distance from the left (or almost equivalently from the right) river boundary provides additional guidance to the DS simulations while looking for patterns in the

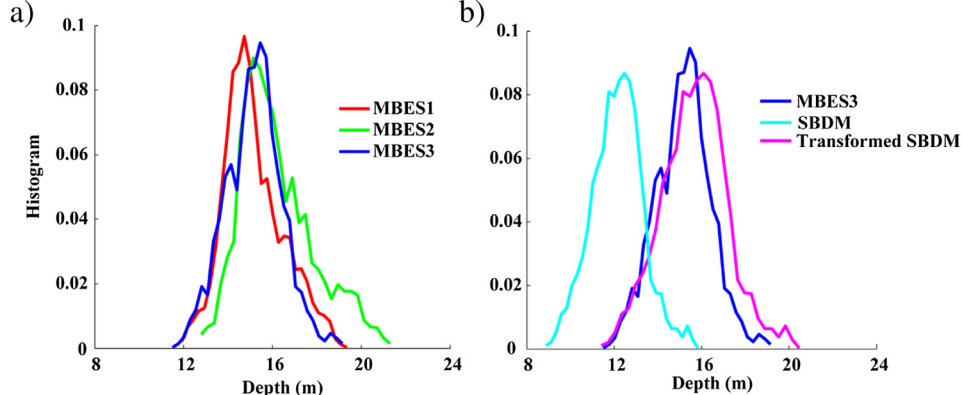


Fig. 2. (a) Histogram of MBES data. (b) Histogram of MBES3 and SBDM data. The affine transformation is applied to SBDM data to obtain transformed SBDM as close as possible to MBES3 data.

Table 1
Statistics of survey data.

Data	Mean	Standard deviation
MBES1	15.14	1.343
MBES2	16.198	1.663
MBES3	15.159	1.251
SBDM	12.143	1.158
Transformed SBDM	15.669	1.503

training image. The effect of the locational variables is to influence the distance used to compare patterns, biasing for a given location the selection of training image patterns from the same area. This way, the non-stationarity observed in the training images can be respected in the simulated domain. In this process, the definition of “same area” needs specific attention.

The process of imposing a local penalty in the DS simulation is illustrated in Fig. 4. Let us consider the simulation of a point in the middle of the river (shown as a star in Fig. 4), with the coordinates of this point denoted as x^* and y^* , and its distance to the left bank denoted as dl^* . The three locational variables considered are x , y and dl . To simulate at the star location, a distance is computed for each locational variable using Eq. (1), resulting in individual distances $d_x = x - x^*$, $d_y = y - y^*$ and $d_{dl} = dl - dl^*$, which are represented on the entire domain in Fig. 4a, b and c. Assuming all weights w_x , w_y and w_{dl} set to 0.1, the component of the distance related to the locational variables is shown in Fig. 4d. In this map the blue areas will tend to be preferentially sampled when simulating the star location. This example shows how the locational variables enforce local consistency: x and y make sure that the sampled patterns are close to the point to be simulated, while dl ensures that the search is preferentially done in the channel direction, taking account of the fact that spatial structures are more continuous along this axis.

Two types of DS simulations are performed: with and without conditioning data, referred here as conditional and unconditional simulations respectively. The rationale behind DS simulations without conditioning data is to check the sensitivity of model parameters for replicating the global bedforms in the river. Once the

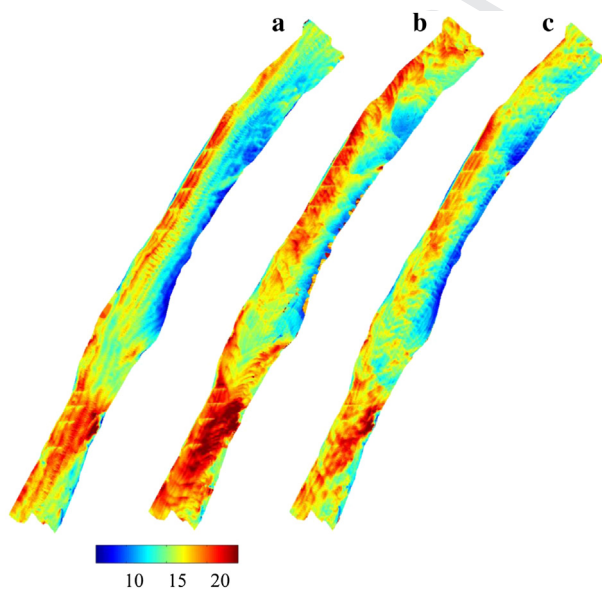


Fig. 3. Training images containing bathymetry measurements from MBES1 (a) and MBES2 (b). MBES3 (c) is shown here only for comparison. The colorbar shows the depth of the river bed in meters. (For interpretation of the references to color in this figure legend, the reader is referred to the web version of this article.)

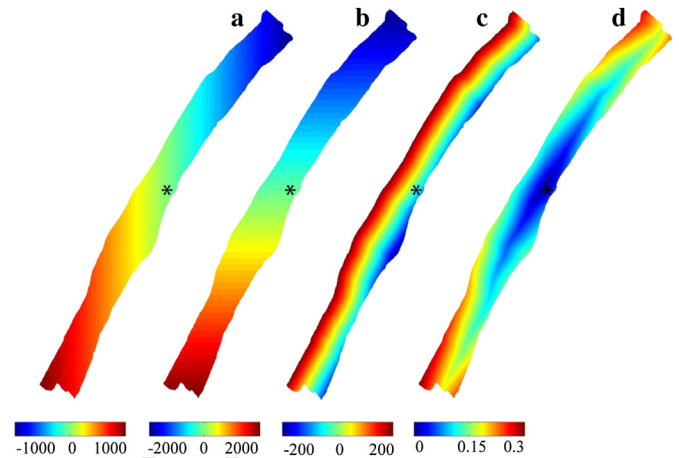


Fig. 4. Maps showing the combined effect of three locational variables (x , y , dl) in constraining the sampling of the training images in the DS simulation. The simulation location is shown in by a star. Difference in x -coordinates (a), in y -coordinates (b), and in dl (c) between the simulation location and all other pixels are shown in the first three figures. (d) Shows the combined distance map with the weights (w_x , w_y and w_{dl}) set to 0.1. In the first three figures the colorbar shows the distances in meters. In the last figure, the colorbar shows the normalized distance value.

spatial structure is adjusted in unconditional mode, we run the conditional DS simulation using conditioning data. From the DS simulations, the expected output is a bathymetry map comparable to that of MBES3 (Fig. 3c), which is used for validation. As discussed in the methodology section, a neighborhood of each variable has to be defined for the DS simulation. Also, each variable is assigned a weight, which is used in the distance calculation (Eq. (2)). There are 4 variables in total (x , y , dl and bathymetry), and the sum of all the variable weights must equal 1.

The main aim is to capture the bedforms correctly, which are expected to change with variation in the assigned neighborhood and weights of the variables. A sensitivity analysis is first performed to determine the weights (w_x , w_y , w_{dl} and $w_{bathymetry}$) corresponding to each variable. The weights are adjusted to obtain the correct spatial variability and features. Quantitative error evaluation is done by estimating the root-mean-squared-errors (RMSE) and relative-mean-squared-errors (Relative MSE) between DS output and both the training images (MBES1 and MBES2). To evaluate the preservation of spatial continuity we compared the omnidirectional variograms produced from DS outputs, with those obtained from MBES data.

The following parameters are kept fixed in all the simulations. The maximum search distance is defined as 50 pixels in the x and y directions. The number of neighboring pixels for the bathymetry considered is 20, which was found to be an appropriate value in previous studies (Meerschman et al., 2013). A single neighbor is assigned for latitude, longitude, and distance from the left bank, which is enough to define the location of a simulation grid point. The distance threshold t is defined as $t = 0.01$, which is the value giving the best results for continuous variable in Meerschman et al. (2013).

The simulation was performed on a grid of 5 m by 5 m resulting in a total 734×1114 pixels. The pixels lying outside the river boundary were masked and not considered for the simulation. Each simulation during the sensitivity analysis consists of 10 realizations to quantify the local probability distribution at each node. The final simulation with conditioning data was run for 100 realizations, which is then used to measure the uncertainty in the results. We also compared the variograms produced from the final simulation results with those produced from MBES3 data.

Table 2
Runs performed for the sensitivity analysis.

w_x, w_y, w_{dl}	RMSE ^a				Relative MSE ^a			
	RMSE1	RMSE2	Average RMSE	RMSE3	Relative MSE1	Relative MSE2	Average relative MSE	Relative MSE3
0	2.225	2.295	2.259	2.169	0.9923	1.0027	0.9975	0.9518
0.02	1.594	1.931	1.762	1.662	0.0137	0.0137	0.0137	0.0151
0.04	1.446	1.977	1.712	1.564	0.0105	0.0122	0.0113	0.0125
0.06	1.329	1.846	1.587	1.5	0.0099	0.0119	0.0109	0.0115
0.08	1.143	1.832	1.487	1.387	0.0093	0.0117	0.0105	0.0115
0.1	1.037	1.829	1.433	1.35	0.0090	0.0112	0.0101	0.0111
0.12	1.226	1.765	1.496	1.444	0.0077	0.0114	0.0095	0.0102
0.14	1.132	1.802	1.467	1.405	0.0075	0.0118	0.0096	0.0102
0.16	1.169	1.693	1.431	1.43	0.0082	0.0115	0.0098	0.0108
0.18	1.171	1.73	1.451	1.423	0.0073	0.0114	0.0093	0.0101
0.2	1.12	1.726	1.423	1.38	0.0076	0.0107	0.0092	0.0100

^a RMSE1, RMSE2, RMSE3, Relative MSE1, Relative MSE2, and Relative MSE3 represent the average value of root-mean-squared error and relative-mean-squared error between each of 10 realizations with MBES1, MBES2 and MBES3 data. Average RMSE is average of RMSE1 and RMSE2. Average Relative MSE is an average of Relative MSE1 and Relative MSE2.

5. Results

5.1. Sensitivity analysis of the weights of locational variables

In a preliminary step we carried out tests to determine the weights of all the variables (w_x , w_y , w_{dl} and $w_{bathymetry}$). These weights reflect the strength of the temporal persistence in the river bed features. Large weights mean that non-stationary high and low values locally observed in MBES1 and MBES2 are expected to remain broadly at the same locations as river bed topography changes. Conversely, small weights mean that the observed features are more stationary and can occur at any location. It should be noted here that when too high weights are used, the DS simulation tends to borrow patterns at the exact same location in the training image, resulting locally in an exact copy of the training image. This phenomenon, called “verbatim copy”, is not desirable because it results in an artificially low variability between realizations.

To assess the influence of the locational variables with a single parameter, we kept the value of w_x , w_y , w_{dl} identical in all the simulation runs, and modified this single value in the sensitivity analysis. As mentioned in Eq. (2), the sum of weights equals 1. Table 2 summarizes the set of runs undertaken for the sensitivity analysis. Each weights value was run for 10 unconditional realizations. Since we are in an unconditional setting, the validation criterion is that the realizations should resemble both MBES1 and MBES2, including reproducing the non-stationary features while showing variability. In a second step, we also use MBES3 (supposedly unknown) to further validate the analysis. Hence for each realization of every run, we calculated the RMSE and Relative MSE between the DS output and both MBES1 and MBES2 data. The RMSE is useful to grasp the absolute magnitude of errors, but it is known to be biased towards extreme values, which are expected to vary in each simulation. Therefore, a Relative MSE was also calculated to quantify the accuracy of the results. RMSE and Relative MSE are obtained using the following formulas (Bennett et al., 2012):

$$RMSE = \sqrt{\frac{1}{n} \sum_{i=1}^n (Z_{i, DS} - Z_{i, MBES})^2} \quad (4)$$

$$Relative\ MSE = \frac{1}{n} \sum_{i=1}^n \left(\frac{Z_{i, DS} - Z_{i, MBES}}{Z_{i, MBES}} \right)^2 \quad (5)$$

where z represents the depth; the subscripts DS and MBES represent the depths obtained from DS simulation and MBES survey data

respectively; i represents a particular pixel and n is the total number of pixels in the simulation grid. Based on average value of RMSE and Relative MSE we decided on an optimum set of weights for the variables used in the final runs with the conditioning (SBDM) data.

Fig. 5 represents the simulation result with single realizations from each run (top row), mean bathymetry of 10 realizations (second row), and corresponding standard deviation (bottom row). Fig. 5a–f correspond to DS output of runs with weights of w_x , w_y , and w_{dl} as: 0.02, 0.06, 0.1, 0.14, 0.18, and 0.2, as listed in Table 2. The effect of increasing weights to x , y and dl (w_x , w_y , w_{dl}) can be clearly seen by comparing Fig. 5a with other figures in the first row. From Fig. 5a, it appears that a small weight on the locational variables is not capable of addressing the non-stationarity in the simulation. We observe that at any given location, the algorithm produces bedforms from everywhere in the training image, which results in homogenized features over larger areas in the bathymetry map. With slightly higher weights in Fig. 5b, the simulations produce global features. By comparing Fig. 5b with the training images in Fig. 3, it can be seen that the global bedforms are correctly reproduced. DS results are able to capture the shallow area on the east bank, deeper areas on the left bank of the river and other deep locations near the bottom part of the river. Some of the bedforms like those in the middle of the reach are correctly reproduced from first training image. This occurs because while searching the similar neighborhood in the training image, DS is guided by not only the latitude and longitude but also by the variable dl , which helps in honoring the bedforms along the river. As the weights of locational variables are increased further to 0.1, all the river training dikes begin to appear in the simulation output as shown in Fig. 5c.

Close comparison of Fig. 5b and c with training images in Fig. 3a and b, shows that the DS output has bedforms coming from both training images. In Fig. 5d, some of the bedforms near the dikes that were nicely reproduced from training images in Fig. 5c disappear and new bedforms appear in the middle and lower portions of the reach. In Fig. 5e, the bottom part of the reach has bedforms very similar to those present in the second training image (Fig. 3b) and similarly the bedforms on the top part of the reach better match the first training image (Fig. 3a). Similar observations also apply to Fig. 5f. The reasons for such behavior in the DS output can be attributed to the fact that large weights assigned to the locational variables (0.2 in Fig. 5f) result in the occurrence of verbatim copy, with different parts of the training images patched together.

These observations are confirmed when comparing the mean and standard deviation maps in Fig. 5, where large values of weights of locational variables lead to low standard deviation and

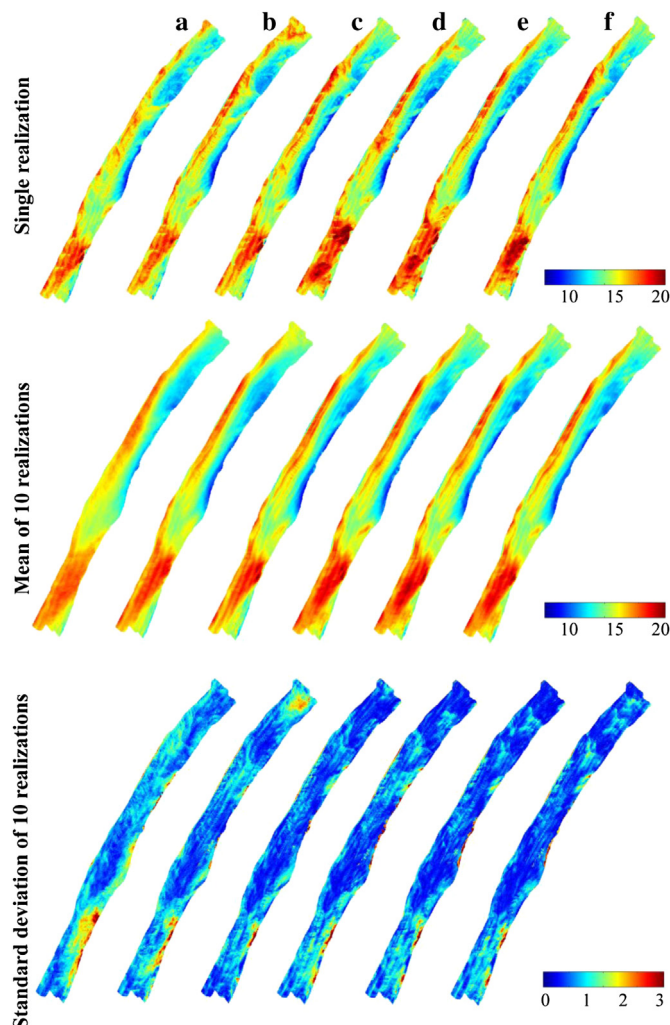


Fig. 5. Bathymetry map produced from sensitivity of weights of locational variables (latitude, longitude, and distance from left bank) in DS simulation runs [a: 0.02; b: 0.06; c: 0.1; d: 0.14; e: 0.18; f: 0.2 respectively]. Single realization of DS output (first row); mean of 10 realizations (second row); and corresponding standard deviation (bottom row) are shown.

therefore low variability/uncertainty in the output bathymetry map.

The quantitative evaluation of the different runs is based on the RMSE and Relative MSE values calculated between the DS realizations and the training images. Ideally the use of the locational variables should yield a general non-stationarity trend that is similar to the one observed in the training images, although the patterns can vary locally. In Table 2, RMSE and Relative MSE represent the average value of RMSE calculated with respect to the training images MBES1, MBES2, and reference MBES3 (Fig. 3a–c respectively). RMSE3 and Relative MSE3 are listed here only for validation, because RMSE3 was not used as training image. These values correspond to the average RMSE and Relative MSE computed using 10 DS realizations. It is expected that the DS simulation captures bedforms from both the training images therefore the individual errors for MBES1 and MBES2 are analyzed separately.

A trade-off has to be found such that the weights of the locational variables are high enough to enforce non-stationary trends, but not too high, otherwise the resulting realizations might show little variability. The average values of RMSE and Relative MSE in Table 2 show that the errors decrease between locational weights of 0 and 0.1. For values higher than 0.1, there is no common trend

observed in the error values, although these higher values do translate into a decreased uncertainty. We therefore use a weight value of 0.1 for the locational variables as it appears to be an appropriate trade-off between a global handling of non-stationarity and accurate reproduction of detailed bedforms features.

The results are further investigated by analyzing the omnidirectional variograms of the simulations. Fig. 6 shows the variograms based on single realizations of DS outputs and also based on the training images (MBES data). As the weights of locational variables are increased from 0 to 0.1, the variogram of the simulations shifts towards the MBES data. The results of runs with weights 0.02 and 0.06 are far from variograms based on MBES data. The variograms of DS output corresponding to runs with weights 0.1, 0.14 and 0.2 are close to each other. Based on this analysis we conclude that weight 0.1 can be considered as optimal for locational variables since further increasing the weights does not improve variogram reproduction. It was therefore decided to use 0.1 as the optimum weight in this study.

5.2. Updating bathymetry using resampled MBES3 data

The objective so far was to find the optimal parameterization of the weights of different variables to capture the global and local scale bedforms correctly. Therefore only training images MBES1 and MBES2 were used without any conditioning data. To accomplish bathymetry fusion, the next step is to integrate the available data corresponding to the medium flow period with the structures observed in MBES1 and MBES2 (low and high flow periods). To investigate the influence of conditioning data on the DS simulation, we carried out analysis using resampled MBES3 data along a zig-zag path (a hypothetical boat route) along the river reach. Since they are extracted from the reference, these conditioning data are deemed unbiased and error-free, however in a real case, high-frequency SBDM data would have reduced accuracy, and would therefore need to be dealt with in a specific manner. This will be further investigated in Section 5.4. For the moment the goal is to evaluate the prediction accuracy using correct conditioning data that correspond to MBES3. The weights on locational variables are set to 0.1 as determined in the previous section. Essentially, the conditional DS simulation then uses bedforms patterns from training images MBES1 and MBES2, and places them at different locations such that they form seamless patterns, but still honor the global trend as well as the data are available along the zig-zag path.

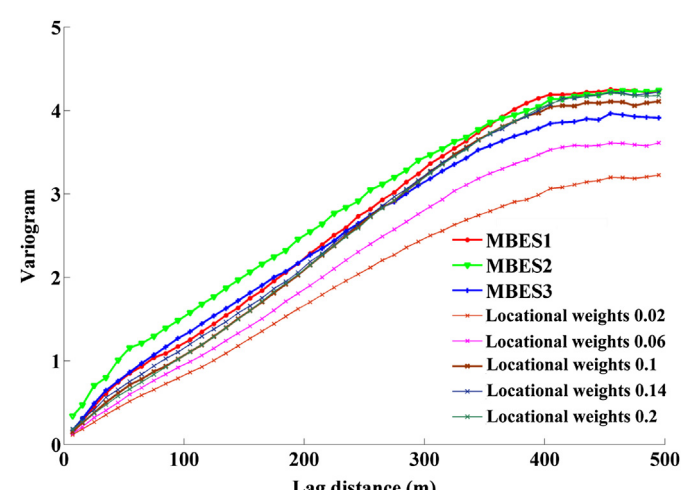


Fig. 6. Variogram of single realization of DS output obtained from sensitivity analysis of weights of locational variables (latitude, longitude, and distance from left bank). The weights of locational variables are shown in the legend.

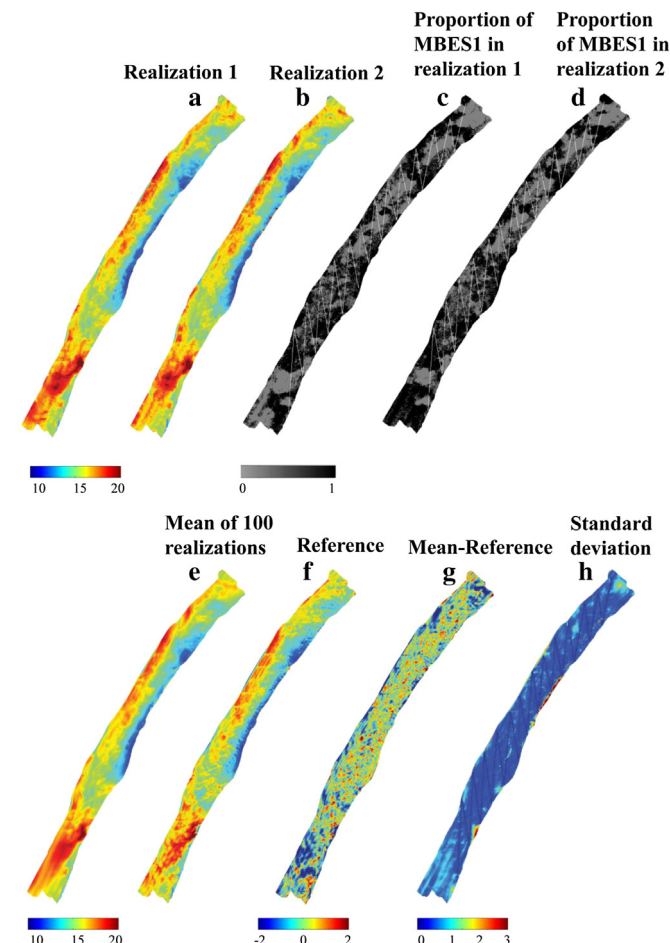


Fig. 7. Bathymetry maps produced from DS simulation runs with weights of locational variables as 0.1. The MBES3 data along a zig-zag boat path has been used as conditioning data. From left to right: results of first two realizations (a and b); proportion of pixels borrowed from MBES1 in two realizations, with black pixels corresponding to MBES1 (c and d); mean of 100 realizations (e); reference map generated from MBES3 data (f); error map showing difference between mean and reference values (g); and standard deviation estimated from 100 realizations of DS output (h). The zig-zag boat path is visible in (c) and (d).

Fig. 7 summarizes the results obtained from 100 realizations with MBES1 and MBES2 as training images, and MBES3 data along the zig-zag path. Fig. 7a and b represent the first two realizations. To visualize how the information from both training images is combined and to assess the occurrence of verbatim copy, we introduce the use of maps indicating the training image of origin for each simulated pixel. Such maps corresponding to the first two realizations are represented in Fig. 7c and d. The black areas indicate pixels originating from MBES1 and the white areas originating from MBES2. Note that even though pixels values are resampled from the training images, the location of these values can vary from the original training image according to the locational weights (see Fig. 7d), hence the result is much more variable than a simple

patchwork of both training images. The proportion of black pixels in these two maps is 52% and 56%, showing that the realizations are a balanced combination of both training images. These maps also demonstrate that verbatim copy does not occur extensively, with the absence of extensive contiguous areas coming from the same training image.

The effect of using conditioning data in the simulation can be seen by comparing Fig. 5c (unconditional simulation corresponding to run with weight 0.1 on locational variables in the sensitivity analysis; it was selected as representing the optimal weights for the locational variables) and the first two maps of Fig. 7. In both figures global bedforms along the left and right banks are similar, but in Fig. 7a and b additional features have appeared. It is also found that deeper regions have appeared on the upper and lower portions of the river. This means that the conditional data have not only affected the locations where they are available (see white lines in Fig. 7c for exact conditioning data locations) but also at other parts of the river.

In the second row of Fig. 7, we present the mean bathymetry of 100 realizations and the corresponding standard deviation. The reference MBES3 data are also shown for comparison. As expected, a low standard deviation is observed not only in the vicinity of the conditioning data but also everywhere in the standard deviation map, with a zero standard deviation at the data location. Fig. 7g shows the average error map, which is the difference between the mean of 100 realizations and the reference MBES3 data. This error is relatively low and evenly distributed, indicating that the global trend is adequately captured. The resulting RMSE and Relative MSE values for the conditional simulations are summarized in Table 3. As expected, we observe that both the RMSE and Relative MSE in conditional simulation using actual reference data along zig-zag path are lower compared to unconditional simulations (see column 2 and 3).

As stated earlier, reproducing the specific patterns of bathymetry can be critical for a range of applications. Therefore, even though the average of the realizations is similar to the reference, we still need to make sure that the simulated patterns are similar to the patterns of the reference. This is done by comparing the variograms of the 100 realizations with the variograms of both training images as well as the reference (Fig. 8). It can also be seen that the conditioning data results in narrowing the spread of variograms around to the reference data MBES3. From these observations, we can conclude that the conditioning data not only affects the local prediction but also affects the spatial structure of the DS output.

5.3. Comparison with a classical detrending approach

The nonstationarity in bedforms was addressed by imposing locational auxiliary variables (latitude, longitude and the distance of data points from the left boundary). In this sense, our method is different from the classical detrending approach which would consist in: (i) computing a common trend from MBES1 and MBES2; (ii) estimating the residuals by subtracting the trend from the training images as well as the conditioning data; (iii) performing the simulation on the residuals; and (iv) adding the trend back to the residual surface (Merwade, 2009). For comparison, we applied

Table 3
Comparison of global errors obtained from 100 realizations of DS simulations.

	Unconditional	Conditional with MBES3 data along zig-zag path	Using classical detrending approach; conditional with MBES3 data along zig-zag path	Conditional with transformed SBDM data	Conditional with MBES3 data at SBDM points
RMSE3 ^a	1.405	1.179	1.227	1.488	1.395
Relative MSE3 ^a	0.0103	0.0075	0.0084	0.0131	0.0108

^a RMSE3 and Relative MSE3 represent root-mean-squared error and relative-mean-squared error between each of 100 realizations and MBES3 data.

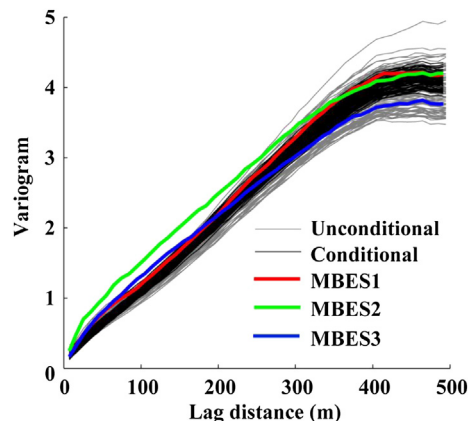


Fig. 8. Variogram of DS outputs obtained from 100 realizations of conditional and unconditional simulations. The conditional and unconditional simulation refers to DS runs with and without zig-zag data. The weights of locational variables (latitude, longitude, and distance from left bank) are kept as 0.1 in all the runs.

this classical detrending approach to perform conditional simulation using the same resampled MBES3 data along a zig-zag path, and compared with the results of the previous section. A moving average of window 50*50 pixels was applied to estimate the trend surface in MBES1 and MBES2 data. The residuals were obtained by removing the average trend from both TIs and also from the conditioning data, and this average trend was added back to the simulation results. The resulting RMSE3 and Relative MSE values were found to be 1.227 and 0.0084, which are higher than the error values obtained with our method, (1.179 and 0.0075 respectively, see columns 3 and 4 of Table 3). It is also worth pointing out that the method of trend estimation and the window size will affect the final results. In our opinion, the proposed method using auxiliary locational variables to impose local consistency is a viable alternative to detrending, and is also straightforward to implement since there is no need for explicit trend estimation.

5.4. Updating bathymetry using SBDM data

To assess our method in a realistic scenario, we used for conditioning data the transformed SBDM obtained from Eq. (3). The parameter values in DS simulation runs are kept the same as previously used in the Section 5.2. The conditional DS simulation is expected to borrow patterns from both training images and locally honor the SBDM data that are available only in a narrow region of the navigation channel.

The results from 100 realizations are summarized in Fig. 9, retaining the same layout as Fig. 7. By comparing the simulation results of first two realizations (Fig. 9a and b) with unconditional realizations (Fig. 5c), it can be observed that additional features have appeared, especially in the middle of the river where the conditioning data are located (Fig. 9c and d indicating exact conditioning data locations). The bedforms are different from those presented in Fig. 7 where spatially distributed data were used along a zig-zag path. The proportion of pixels coming from Fig. 9c and d are 44% and 39% respectively, indicating that the amount of pixels originating from MBES1 depends on the location of the conditioning data. In this case, the very sparse SBDM data happen to better correspond to training image MBES1, showing that sampling only the deeper areas along a navigational path is not optimal. In this case again, extensive verbatim copy does not occur.

By comparing the mean value of 100 realizations (Fig. 9e) with the reference MBES3 data (Fig. 9f), it can be observed that the DS simulation is not able to capture some of the features present on

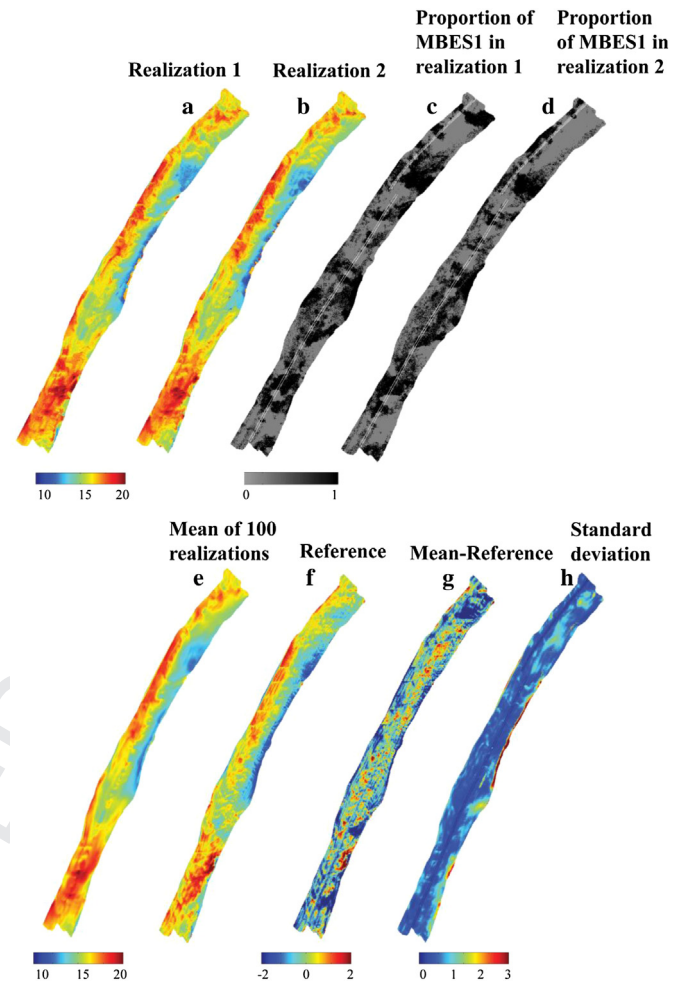


Fig. 9. Bathymetry maps produced from DS simulation runs with weights of locational variables as 0.1. The SBDM data has been used as conditioning data. From left to right: results of first two realizations (a and b); proportion of pixels borrowed from MBES1 in two realizations, with black pixels corresponding to MBES1 (c and d); mean of 100 realizations (e); reference map generated from MBES3 data (f); error map showing difference between mean and reference values (g); and standard deviation estimated from 100 realizations of DS output (h). The SBDM data locations are visible in (c) and (d).

the right bank of the river (in blue color). The error map in Fig. 9g also shows nonzero error at the conditioning data locations, which emphasizes the drawbacks of the affine transformation (Eq. (3)) performed on the SBDM data, and therefore does not result in the SBDM locally matching MBES3. This error is inherent to the different measurement methods used, SBDM being less accurate than MBES, and this is the reason why we transformed SBDM data into the space of MBES and not the opposite. The standard deviation map (Fig. 9h) shows a zero standard deviation at the data location and a reduced variability in the vicinity of the conditioning data.

The RMSE and Relative MSE between each of the 100 DS realizations and the reference MBES3 data are shown in Table 3. The mean RMSE and Relative MSE of all realizations are higher than what was observed in the unconditional case (see columns 2 and 5). One factor that explains this discrepancy is the differences in values obtained by the different measurement techniques, and the resulting imperfect affine transformation. Another factor is that the non-stationary features of MBES1 and MBES2 may not be compatible with the conditioning data, therefore causing a large mismatch in regions away from the navigation channel.

Table 4
Comparison of local errors obtained from 100 realizations of DS simulations.

	Unconditional	Conditional with transformed SBDM data	Conditional with MBES3 data at SBDM points
RMSE3 ^a	1.321	0.843	0.483
Relative MSE3 ^a	0.007992	0.003122	0.001077

^a RMSE3 and Relative MSE3 represent root-mean-squared error and relative-mean-squared error between each of 100 realizations and MBES3 data.

To further investigate the influence of discrepancy in transformed SBDM data on the DS simulation, we used the actual, error-free reference MBES3 data considered only at the SBDM locations. The idea behind this approach is to evaluate the effect of the data bias and to estimate how much improvement can be achieved by using correct conditioning data that correspond to MBES3. The resulting RMSE and Relative MSE values are summarized in Table 3. By comparing the error values in the fifth and sixth columns of Table 3, we observe a significant reduction in errors. This observation indicates that if the SBDM were unbiased, it would be possible to use them to obtain a more accurate bathymetry update.

To estimate the local improvement in conditional simulations, an area covering a 20 m radius around the SBDM data locations was defined. We calculated the RMSE and Relative MSE between the reference data (MBES3) and the DS simulations for this area only. The resulting error values are presented in Table 4, where it can be seen that at a local level, conditional simulation even with transformed SBDM data shows much improvement over unconditional simulation. Further improvement is observed when unbiased data are used. This local improvement is explained by the high spatial variability of the river bathymetry. It can be concluded that the SBDM data can bring local improvement, but is not useful for predicting the global evolution of the bathymetry beyond the correlation range of the spatial variability of the bedforms features.

6. Conclusion

In this study we demonstrate the application of the Direct Sampling (DS) multiple-point geostatistical method for applications to bathymetry fusion, in particular to update estimates of river bathymetry based on high-frequency, low-cost measurements. The DS algorithm determines the value of each pixel by sampling training images and conditioning the outcome to the available data. To our knowledge, it is the first application of multiple-point geostatistics where several equally probable alternative training images are mixed to represent different spatial scenarios.

The training images used represent two extreme stages of the river bathymetry (high and low flow) obtained by high-resolution MBES surveys, hence spanning the range of spatial patterns expected under medium flow conditions. It should be noted that our approach could also be applied with training images obtained from adjacent river reaches that present similar bathymetry characteristics. Low-cost SBDM data, obtained along boat paths in a medium-flow stage, are used as conditioning data. Geostatistical simulations were performed that represent predictions of high-resolution bathymetry for medium-flow. These results are validated using exhaustive reference MBES data taken during medium flow conditions. The SBDM data are available along a boat path, providing only sparse coverage of the river, and moreover present significant bias.

Different scenarios were considered, using unbiased data (sampled from the reference) and transformed SBDM data, and different sampling designs were considered (zig-zag or maximum depth navigational path). It is observed that large spatial data

coverage is necessary in order to capture bathymetry features on a non-stationary domain, indicating it is not sufficient to use data only along commonly used navigational channels.

The non-stationarity of bedforms is dealt with by an approach involving the use of locational variables, which proves to be at least as efficient as a classical methodology involving trend modeling. Although systematic bias is observed between MBES and SBDM surveys, the updated bathymetry from DS simulations shows good agreement with the reference in the vicinity of the boat data. Further improvement is observed locally when using unbiased data. The present findings demonstrate the potential of the DS approach for bathymetry fusion and creating an updated bathymetry map, as a cost-effective alternative option to performing periodic detailed survey of bathymetry in large rivers.

Acknowledgments

The data used in this research were collected and analyzed by a team of researchers during the post-doctoral research fellowship awarded to first author at the National Center for Supercomputing Applications, Illinois, USA. The application of the new approach presented in this paper was supported through a post-doctoral research fellowship as part of the National Center for Groundwater Research and Training (NCGRT), a joint initiative between the Australian Research Council and the National Water Commission.

References

- Alcântara, E., Novo, E., Stech, J., Assireu, A., Nascimento, R., Lorenzetti, J., Souza, A., 2010. Integrating historical topographic maps and SRTM data to derive the bathymetry of a tropical reservoir. *J. Hydrol.* 389 (3), 311–316.
- Arpat, B.G., Caers, J., 2007. Stochastic simulation with patterns. *Math. Geol.* 39 (202), 177–203.
- Bailly, J.S., Le Coarer, Y., Languille, P., Stigtermark, C.J., Allouis, T., 2010. Geostatistical estimations of bathymetric LiDAR errors on rivers. *Earth Surf. Proces. Landf.* 35 (10), 1199–1210.
- Barnes, R., Watson, A., 1992. Efficient updating of kriging estimates and variances. *Math. Geol.* 24 (1), 129–133.
- Bennett, N.D., Croke, B.F., Guariso, G., Guillaume, J.H., Hamilton, S.H., Jakeman, A.J., Marsili-Libelli, S., Newham, L.T., Norton, J.P., Perrin, C., 2012. Characterising performance of environmental models. *Environ. Model. Softw.*
- Boucher, A., Kyriakidis, P.C., Cronkite-Ratcliff, C., 2008. Geostatistical solutions for super-resolution land cover mapping. *IEEE Trans. Geosci. Remote Sens.* 46 (1), 272–283.
- Calder, B., 2006. On the uncertainty of archive hydrographic data sets. *IEEE J. Ocean. Eng.* 31, 249–265.
- Carter, G.S., Shankar, U., 1997. Creating rectangular bathymetry grids for environmental numerical modelling of gravel-bed rivers. *Appl. Math. Model.* 21 (11), 699–708.
- Chappell, A., Heritage, G.L., Fuller, I.C., Large, A.R.G., Milan, D.J., 2003. Geostatistical analysis of ground-survey elevation data to elucidate spatial and temporal river channel change. *Earth Surf. Proces. Landf.* 28 (4), 349–370.
- Chugunova, T., Hu, L., 2006. Multiple-point Statistical Simulations Constrained by Continuous Auxiliary Data. *Int. Assoc. for Mathematical Geology XIth International Congress: Université de Liège, Belgium.*
- Coleman, J.B., Yao, X., Jordan, T.R., Madden, M., 2011. Holes in the ocean: filling voids in bathymetric lidar data. *Comput. Geosci.* 37 (4), 474–484.
- Costa, B., Battista, T., Pittman, S., 2009. Comparative evaluation of airborne LiDAR and ship-based multibeam SONAR bathymetry and intensity for mapping coral reef ecosystems. *Remote Sens. Environ.* 113 (5), 1082–1100.
- Cutter, G., Rzhano, Y., Mayer, L., 2003. Automated segmentation of seafloor bathymetry from multibeam echosounder data using local Fourier histogram texture features. *J. Exp. Mar. Biol. Ecol.* 285, 355–370.
- Elmore, P., Steed, C.A., 2008. Algorithm Design Study for Bathymetry Fusion-review of Current State-of-the-art and Recommended Design Approach (DTIC Document).
- Feyen, L., Caers, J., 2006. Quantifying geological uncertainty for flow and transport modeling in multi-modal heterogeneous formations. *Adv. Water Res.* 29 (6), 912–929.
- Fonstad, M.A., Marcus, W.A., 2010. High resolution, basin extent observations and implications for understanding river form and process. *Earth Surf. Proces. Landf.* 35 (6), 680–698.
- Fuller, I., Basher, L., 2012. Riverbed digital elevation models as a tool for holistic river management: Motueka River, Nelson, New Zealand. *River Res. Appl.*
- Furnans, J., Austin, B., 2008. Hydrographic survey methods for determining reservoir volume. *Environ. Model. Softw.* 23 (2), 139–146.

- Gesch, D., Wilson, R., 2002. Development of a seamless multisource topographic/bathymetric elevation model of Tampa Bay. *Mar. Technol. Soc. J.* 35 (4), 58–64.
- Gómez-Hernández, J.J., Wen, X.H., 1998. To be or not to be multi-Gaussian? A reflection on stochastic hydrogeology. *Adv. Water Res.* 21 (1), 47–61.
- Gooseff, M.N., Anderson, J.K., Wondzell, S.M., LaNier, J., Haggerty, R., 2006. A modelling study of hyporheic exchange pattern and the sequence, size, and spacing of stream bedforms in mountain stream networks, Oregon, USA. *Hydrol. Proces.* 20 (11), 2443–2457.
- Goovaerts, P., 1997. *Geostatistics for Natural Resources Evaluation*. Oxford University Press, USA.
- Guardiano, F., Srivastava, R.M., 1993. Multivariate geostatistics: beyond bivariate moments. *Geostat-troia* 1, 133–144.
- Honarkhah, M., Caers, J., 2010. Stochastic simulation of patterns using distance-based pattern modeling. *Math. Geosci.* 42 (5), 487–517.
- Jena, B., Kurian, P., Swain, D., Tyagi, A., Ravindra, R., 2012. Prediction of bathymetry from satellite altimeter based gravity in the Arabian Sea: mapping of two unnamed deep seamounts. *Int. J. Appl. Earth Obs. Geoinform.* 16, 1–4.
- Jerosch, K., 2012. Geostatistical mapping and spatial variability of surficial sediment types on the Beaufort Shelf based on grain size data. *J. Mar. Syst.*
- Jha, S., Bailey, B., Minsker, B., Cash, R., Best, J., 2011. Updating River Bathymetry with Multiple Data Sources Using Kriging. *American Geophysical Union*, p. 1329.
- Jha, S.K., Mariethoz, G., Evans, J.P., McCabe, M.F., 2013. Demonstration of a geostatistical approach to physically consistent downscaling of climate modeling simulations. *Water Res. Res.* 49, 245–259.
- Jiang, C., Li, J., de Swart, H.E., 2011. Effects of navigational works on morphological changes in the bar area of the Yangtze Estuary. *Geomorphology* 139–140, 205–219.
- Journel, A., Zhang, T., 2006. The necessity of a multiple-point prior model. *Math. Geol.* 38 (5), 591–610.
- Journel, A.G., Huijbregts, C.J., 1978. *Mining Geostatistics*. Academic Press.
- Legleiter, C., 2012. Mapping river depth from publicly available aerial images. *River Res. Appl.*
- Legleiter, C.J., Kyriakidis, P.C., 2008. Spatial prediction of river channel topography by kriging. *Earth Surf. Proces. Landf.* 33 (6), 841–867.
- Legleiter, C.J., Roberts, D.A., 2009. A forward image model for passive optical remote sensing of river bathymetry. *Remote Sens. Environ.* 113 (5), 1025–1045.
- Liu, X., Parker, G., Czuba, J., Oberg, K., Best, J., 2012. Sediment mobility and armoring analysis of the St. Clair River. *Earth Surf. Proces. Landf.* (in press).
- Mantas, V., Pereira, A., Neto, J., Patrício, J., Marques, J., 2011. Monitoring estuarine water quality using satellite imagery. The Mondego river estuary (Portugal) as a case study. *Ocean Coast. Manag.* 72, 13–21.
- Mariethoz, G., Kelly, B.F.J., 2011. Modeling complex geological structures with elementary training images and transform-invariant distances. *Water Res. Res.* 47 (7), W07527.
- Mariethoz, G., McCabe, M.F., Renard, P., 2012. Spatiotemporal reconstruction of gaps in multivariate fields using the direct sampling approach. *Water Resour. Res.* 48 (10).
- Mariethoz, G., Renard, P., Straubhaar, J., 2010. The direct sampling method to perform multiple-point geostatistical simulations. *Water Resour. Res.* 46 (11), W11536.
- Masetti, G., Calder, B., 2012. Remote identification of a shipwreck site from MBES backscatter. *J. Environ. Manag.* 111, 44–52.
- Meerschman, E., Pirot, G., Mariethoz, G., Straubhaar, J., Van Merivenne, M., Renard, P., 2013. A practical guide to performing multiple-point geostatistical simulations with the direct sampling algorithm. *Comput. Geosci.* 52, 307–324.
- Merwade, V., 2009. Effect of spatial trends on interpolation of river bathymetry. *J. Hydrol.* 371 (1–4), 169–181.
- Merwade, V.M., Maidment, D.R., Goff, J.A., 2006. Anisotropic considerations while interpolating river channel bathymetry. *J. Hydrol.* 331 (3), 731–741.
- Quinn, R., Boland, D., 2010. The role of time-lapse bathymetric surveys in assessing morphological change at shipwreck sites. *J. Archaeol. Sci.* 37 (11), 2938–2946.
- Shelley, J., Abraham, D., McAlpin, T., 2013. Removing systemic bias in bed-load transport measurements in large sand-bed rivers. *J. Hydraul. Eng.* (in press).
- Simmons, S., Parsons, D., Best, J., Malzone, C., Keevil, G., 2007. Measurement of Large-scale Sediment Transport Dynamics Using Multibeam Sonar. *AGU Fall Meeting*, p. 892.
- Sindhu, B., Suresh, I., Unnikrishnan, A., Bhatkar, N., Neetu, S., Michael, G., 2007. Improved bathymetric datasets for the shallow water regions in the Indian Ocean. *J. Earth Syst. Sci.* 116 (3), 261–274.
- Straubhaar, J., Renard, P., Mariethoz, G., Froidevaux, R., Besson, O., 2011. An improved parallel multiple-point algorithm using a list approach. *Math. Geosci.* 1–24.
- Strebelle, S., 2002. Conditional simulation of complex geological structures using multiple-point statistics. *Math. Geol.* 34 (1), 1–21.
- Stumpf, R.P., Holderied, K., Sinclair, M., 2003. Determination of water depth with high-resolution satellite imagery over variable bottom types. *Limnol. Oceanogr.* 547–556.
- Wozencraft, J., Millar, D., 2005. Airborne lidar and integrated technologies for coastal mapping and nautical charting. *Mar. Technol. Soc. J.* 39 (3), 27–35.
- Zhang, T., 2006. *Filter-based Training Pattern Classification for Spatial Pattern Simulation*. Stanford University.